$M_3M_{45}M_{45}$ Auger lineshape measured from the Cu(111) surface: Multiplet term selectivity in angle-resolved Auger-photoelectron coincidence spectroscopy

R. Gotter,[1] F. Da Pieve,[2,*] F. Offi,[2] A. Ruocco,[2] A. Verdini,[1] H. Yao,[3] R. Bartynski,[3] and G. Stefani[2]
[1]*Laboratorio Nazionale TASC-INFM-CNR, Area Science Park, SS 14-km 163.5, I-34012 Basovizza, Trieste, Italy*
[2]*Dipartimento di Fisica and CNISM, Università Roma Tre, Via della Vasca Navale 84, I-00146 Rome, Italy*
[3]*Department of Physics and Astronomy and Laboratory for Surface Modification, Rutgers University, 136 Frelinghuysen Road, Piscataway, New Jersey 08854, USA*

(Received 18 April 2008; revised manuscript received 9 January 2009; published 10 February 2009)

The capability of the recently observed dichroic effect in angle-resolved Auger-photoelectron coincidence spectroscopy (DEAR-APECS) to disentangle individual multiplet terms has been exploited to study the lineshape of the $M_3M_{45}M_{45}$ Auger spectrum measured in coincidence with the $3p_{3/2}$ photoelectrons from the Cu(111) surface. The relevant multiplet structure of the two hole final state is determined with an unprecedented sensitivity, including a reliable experimental estimation of the energy of the ^1D multiplet term. Spectroscopic data for the $3p$ photoemission feature are also given and energy conservation applied to the photoelectron-Auger-electron pair has been successfully used in order to quantitatively explain energy shifts in coincidence spectra. Multiple-scattering calculations prove that the DEAR-APECS effect is not destroyed by diffraction effects and a simple model which combines atomic angular distributions and electron-diffraction modulations is provided in order to obtain a detailed understanding of the multiplet energy and intensity distributions in Auger spectra.

DOI: 10.1103/PhysRevB.79.075108 PACS number(s): 79.60.−i, 78.70.−g

I. INTRODUCTION

Owing to continuing developments in experimental techniques[1,2] and the emergence of reliable *ab initio* calculations,[3] Auger-electron spectroscopy (AES) (Ref. 4) has become a valuable tool to investigate the local electronic structure of solids. Efforts to describe the lineshapes of the Auger transitions of Cu have been critical to gain an understanding of core-valence-valence (CVV) Auger spectra of strongly correlated systems. Several seminal papers of the early 1970s showed that it is necessary to consider both the atomic character[5] as well as the role of solid-state effects, such as the large extra-atomic relaxation,[6] to explain both relative intensities and absolute kinetic energies of features in Cu CVV Auger spectra. Nevertheless the correct assignment of multiplet terms, as well as the evaluation of the widths of the involved hole states, remained controversial for a long time.[7] As a matter of fact, the presence of Auger vacancy satellite structures[8] recognized as Coster-Kronig (CK) preceded decays, which are superimposed on the $L_3M_{45}M_{45}$ Auger decay and the overlap between the M_2 and the M_3 contributions in the $M_{23}M_{45}M_{45}$ decay, are the main limiting factors in interpreting such Auger lineshapes. During the 1970s, configuration-interaction calculations performed for Cu L- and M-shell Auger decays[9] successfully described nonradiative decays involving core-level electrons. In contrast, attempts to model the lineshape of the Cu CVV Auger transitions using an approach based on self-convolutions of one-particle density of states (DOS), eventually including Auger matrix element corrections, gave a poor description of these transitions. This lead to the conclusion that independent-particle-based models are insufficient to describe these Auger transitions in the solid Cu.[10] Indeed, only when the effective correlation energy of the two holes in the Auger final state was taken into account,[11] were all of the principal and satellite Auger spectra carefully calculated in the atomic framework.[12] In that work it was noted that in Cu, as well as in Zn, CK processes are a solid-state effect because they do not occur in the gas phase.[13] At the end of the 1970s, the development of the Cini-Sawatzky (CS) model[14,15] and the introduction of the novel experimental technique of Auger-photoelectron coincidence spectroscopy (APECS) (Ref. 16) gave a deep insight in CVV Auger lineshapes. The CS model was able to explain how electron correlation in the two hole final state affects the independent electron description of CVV Auger spectra and how the strength of this effect depends on the ratio of the Coulomb repulsion energy between the two final holes and the width of the valence band in which those holes are created. In essence, this single description allowed for a continuous interpolation between bandlike and atomiclike Auger decays. Experimental advances, particularly the advent of synchrotron-radiation sources, created a renewed interest in the understanding of the CVV Auger lineshapes as it introduced the possibility to tune the photon energy. By studying the evolution of the Cu $L_{23}M_{45}M_{45}$ spectrum as the photon energy moves through the L_{23} absorption edges, the relative contributions of decay channels arising from CK and initial-state shake-up processes have been estimated.[17] In addition, the relevance of shake-up transitions accompanying the L_3 photoionization process when going from elemental Cu to the more strongly correlated oxide system CuO has been assessed.[18] Moreover, similar to what has been observed for Ag, a progressive skewing of the lineshape at the expense of the ^1G intensity, as the photon energy moves below the L_3 threshold,[19] has been attributed to DOS effects in the vicinity of the Fermi level.[20,21]

In the APECS technique, the kinetic-energy distribution of Auger electrons is detected in time coincidence with the precursor photoelectrons generated in the production of the

Auger initial state. When first applied to the CVV Auger transitions of Cu, APECS enabled discrimination between CK and diagrammatic transitions (originating from different core-hole states), even though there is a substantial overlap in energy among these transitions.[16] When coupled with high-energy resolution and variable photon energy of synchrotron-radiation sources, APECS also permitted the study of Auger transitions with an energy resolution beyond natural lifetime limits,[22] with an inherently high-surface sensitivity,[23] and even with the possibility to select the average emission depth within a range of few atomic layers.[24] An important recent advance of the APECS technique consists in detecting the Auger-electron-photoelectron pairs correlated in angle as well as in energy and time that is performing an angle-resolved APECS (AR-APECS) experiment. The feasibility of AR-APECS from solids has been demonstrated by pioneering work on the Cu(111) surface.[25] In a subsequent investigation on the Ge(100) surface, it was found that the angular distribution of Auger electrons measured in coincidence with the precursor photoelectron depends upon the emission direction of the detected photoelectron. These findings suggested that measuring angular-resolved coincident Auger-photoelectron pairs amounts to observing Auger decays originating from core-hole states whose polarization can be specified by defining the mutual directions of the light polarization and momentum vectors of the two emitted electrons.[26] In a similar way, when an AR-APECS experiment is performed by fixing the detection angle of both electrons, the coincidence Auger energy distribution depends upon the ejection angle of the coincident photoelectron. Such a dependence arises because the dipole and Coulomb selection rules jointly determine the relative abundance of the multiplet components in the observed Auger spectrum. Indeed, the ability to manipulate the relative contributions to the AR-APECS spectrum from electronic sublevels characterized by a different quantum numbers amounts to a geometry-induced dichroic effect on final-state spins that contribute to the coincidence Auger energy spectrum. Experimental evidence for the presence of such a dichroic effect in angle-resolved-APECS (DEAR-APECS) has been reported for a 1/3 atomic layer thick Sn film deposited on the Ge(111) surface.[27] In that experiment the submonolayer range was chosen in order to focus on the atomic origins of this effect and to avoid electron-diffraction effects related to the presence of a crystal lattice. As a matter of fact, those results resemble dichroic effects observed in similar coincidence experiments on free atoms either by changing the initial atomic polarization[28] or by changing the light polarization[29,30] (even if the magnetic sublevels are not resolved).

The aim of the present work is to apply the enhanced capability of DEAR-APECS to perform a detailed spectroscopic study of the otherwise unresolved multiplet terms in the Cu $M_{23}M_{45}M_{45}$ Auger spectrum from the Cu(111) surface. By exploring the influence of DEAR-APECS on relative intensities of the multiplet structures, we give quantitative evidence for energy conservation experienced by the coincident Auger-photoelectron pair. With input from photoelectron-diffraction simulations, we demonstrate that the DEAR-APECS effect remains strong even when the emitted electrons in the coincidence pair undergo significant diffraction within the crystal. Results will be interpreted with the help of a simple atomic model in which autoionization described in *LS* coupling is followed by diffraction from the crystal lattice for each electron in the coincidence pair. By using different relative orientations of the light polarization and the emission directions of each detected electron in the pair, we have been able to increase or reduce the relative intensities of the ^1G, ^1D, and ^3F components of the $M_3M_{45}M_{45}$ coincidence Auger spectrum. The results suggest that due to the DEAR-APECS effect, even a modest restriction on emission angles plays an important role in determining the relative intensities of the multiplet terms. A more complete theoretical treatment of the DEAR-APECS effect would enable more precise connection with predicted solid-state properties and, since multiplet term selectivity can be easily associated to selectivity in the spin final state, would provide an alternative way to study magnetic systems.[31] Finally, we also present conventional (singles) x-ray photoemission spectroscopy (XPS) as well as AES spectra to provide a quantitative comparison between conventional and coincidence Auger spectroscopies and to assemble a comprehensive data set for the Cu $3p$ photoemission and the $M_3M_{45}M_{45}$ Auger decay spectra.

II. EXPERIMENTAL

Experiments were performed at the ALOISA beamline of the ELETTRA synchrotron-radiation facility in Trieste (Italy). The apparatus is discussed in detail elsewhere[32] and only a brief description will be given here. We used for our investigation a Cu(111) single crystal cleaned by cycles of sputtering and annealing until surface contaminants were below the detection limit of photoemission spectroscopy and until a well-ordered surface was obtained, as verified by reflection high-energy electron diffraction. Monochromatic radiation of energy $h\nu=241$ eV in a nearly p polarization condition impinged on the Cu(111) surface at a grazing incidence angle of about 6°, where the surface normal lies in the plane determined by the photon beam direction and the polarization vector ϵ. The experimental chamber contained seven hemispherical analyzers mounted on either of two rotating frames. Two of the analyzers mounted 18° apart are on an array termed bimodal frame, rotating around the photon beam axis and around an axis normal to it. The other five analyzers (each 18° apart from the next) are positioned on a plane (axial frame) containing the photon beam axis and rotating around it. The bimodal analyzers, with an energy resolution of 2.16 eV, were tuned to a fixed kinetic energy ($E_k=157.8$ eV) corresponding to the high kinetic-energy side of the $3p$ photoemission spectrum. These parameters were chosen in order to efficiently collect the $3p_{3/2}$ component ($E_k=156.8$ eV) only, while avoiding detecting photoelectrons coming from ionization of $3p_{1/2}$ shell. The axial analyzers, with a resolution of 0.9 eV, sampled the energy range of the Auger spectrum. Electrons passing through the analyzers were detected by channeltrons, which produce pulses that were recorded in coincidence with an ultimate timing resolution of $\Delta t \approx 3$ ns, defined by the flight time

dispersion of the electrons inside the analyzers. As usual, the chosen experimental setup is the best compromise—in terms of energy resolution, time resolution, and detection efficiency—in order to get reliable data in reasonable acquisition times.[33] Conventional Auger spectra were also acquired simultaneously during the AR-APECS measurements. Ten simultaneous coincidence spectra were obtained by separately recording events detected in either one of the bimodal analyzer in coincidence with the counts received in any of the axial analyzer. In order to improve the statistical uncertainty, spectra presented in Sec. III have been obtained by adding up APECS events originating from several time-correlated axial-bimodal pairs that were arranged in similar geometrical conditions. The angular degrees of freedom of the analyzer frames allow measurement in different experimental geometries that correspond to different selection on the core-hole polarization and thus on the multiplet terms of the two hole final state. For the experiments presented here we used two configurations. The first configuration (in the following referred to as condition *AN*) has one electron of the pair (the photoelectron detected with the bimodal frame along the surface normal) aligned (*A*) with ϵ, while the other (the Auger electron collected with the axial frame at more than 40° from surface normal) was not aligned (*N*) with ϵ (see Fig. 4 for the exact polar position of the analyzers). In the second geometry (in the following referred to as condition *AA*) most analyzers of both the axial and the bimodal frames were close to the surface normal (at angles mainly $\leq 20°$), and thus they can be considered aligned (*A*) with the polarization direction of the light (ϵ). In this last case, only the two analyzers located at the extremes of the axial frame cannot be considered as aligned, so the respective pairs involving these analyzers have been included in spectra representing the *AN* condition.

III. RESULTS

The Cu $3p$ photoemission and the Cu $M_{23}M_{45}M_{45}$ conventional Auger (from now on referred to as "singles") spectra collected at normal emission and with a higher resolution than the coincidence measurements are reported in Figs. 1(a) and 1(b), respectively. The $3p$ photoemission spectrum (open circles) in Fig. 1(a) has been fitted with two Voigt functions corresponding to the two spin-orbit (SO) split components. The Lorentzian contributions are shown as dashed lines: binding energy 74.72 ± 0.05 eV ($3p_{3/2}$), full width at half maximum (FWHM) 2.06 ± 0.04 eV and 2.05 ± 0.07 eV for the $3p_{3/2}$ and the $3p_{1/2}$ components, respectively, SO splitting 2.50 ± 0.03 eV, and branching ratio (BR) of 0.45 ± 0.02. The FWHM of the Gaussian broadening has been constrained to be equal or larger than the electron analyzer energy resolution of 0.9 eV. The obtained value of 0.93 ± 0.03 eV takes into account for other Gaussian broadening sources such as the photon energy resolution and thermal vibrations. The best fit is superimposed to the experimental points as a solid line, while the dash-dotted line represents a Shirley-type integral background. While binding energies and linewidths are in agreement with previous results, the SO splitting needs some comment. The value of

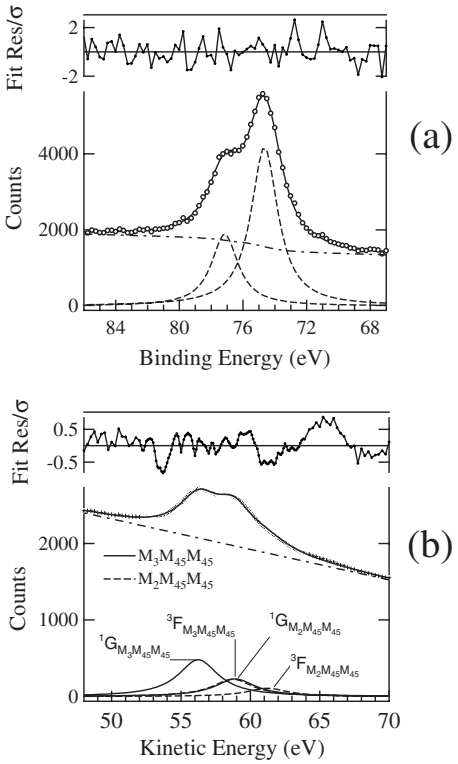

FIG. 1. (a) Cu $3p$ photoemission spectrum (open circles). The solid line is the result of the best fit of the experimental spectrum obtained by using a Shirley-type integral background (dash-dotted line) and two Lorentzian functions (dashed lines) representing the two SO split components which have been convoluted by the experimental Gaussian broadening. (b) Single Cu $M_{23}M_{45}M_{45}$ Auger spectrum (dots with error bars) and best fit (solid line) obtained by the convolution of the experimental Gaussian broadening with four Lorentzian functions representing the multiplet contributions of the M_3 decay (solid line) and the M_2 decay (dashed line). Dash-dotted line is the background. Residuals relative to the error bars σ of each data point are shown in the top part of both panels.

this splitting has been estimated to be 2.3 eV for atomic Cu,[34] 2.2 eV on evaporated Cu,[35] and 2.39 eV on scraped crystal.[36] Very few measurements have been carried out on annealed surfaces of single crystals. The value reported from a Cu(001) surface is 2.2 eV,[37] while the spectrum shown in the angle-resolved study on the Cu(111) surface by Huff *et al.*[38] seems to give a value very close to our result. As a matter of fact, the lifetime widths also seem to have larger values when going from atoms or evaporated Cu to single crystals.[22] The larger width has been attributed to a larger overlap between $3p$ and $3d$ levels, which results in very rapid Auger decay and large lifetime broadened peaks. The small deviation from the statistical population value of 0.5 of the observed BR between the $3p_{1/2}$ and the $3p_{3/2}$ photoemission peaks (0.45 ± 0.02) cannot be attributed to the presence of super Coster-Kronig decays because the linewidth of the two peaks is almost identical, indicating that there is not a sizable extra abundance of decays available for the $3p_{1/2}$ core hole. Such a small discrepancy is instead consistent with anisotropy effects that can be due to both inherent differences in the wave functions (radial parts and phase shifts)[39]

or different interference effect due to the different kinetic energies.[40] A dominant effect of the latter motivation is more reasonable for the present case because we observed that the angular distribution of Cu $3p$ photoelectrons, in the range of the used kinetic energies, is very sensitive to energy changes as small as 2 eV.

In Fig. 1(b) the experimental high-resolution Auger spectrum (dots with error bars) has been fitted with Voigt functions attributed to the more relevant individual multiplet terms of the Auger transition, taking into account natural lifetime and experimental resolution broadening. The overall experimental response function is assumed to be Gaussian in shape and with a FWHM equal to the experimental energy resolution of the analyzers (0.18 eV), while the Lorentzian widths have been forced to be equal for all Auger peaks, being the core-hole lifetime the main broadening source. For the Cu $M_{23}M_{45}M_{45}$ Auger final state, the multiplet terms describing the two holes in the initially filled d band are the singlets ^1G, ^1D, and ^1S and the triplets ^3F and ^3P.[41] Only the more intense terms[2,9,11,42] have been here considered, namely, the ^1G and the ^3F, both for the $M_2M_{45}M_{45}$ (dashed lines) and the $M_3M_{45}M_{45}$ (solid lines) transitions. The CK preceded $M_3M_{45}-M_3M_{45}M_{45}$ Auger vacancy satellite transition has not been considered because it would contribute with another set of peaks very close to the $M_3M_{45}M_{45}$ peaks with an energy separation from this former too small if compared with the Lorentzian broadening. In addition, as was found in previous APECS measurements, the CK decay does not contribute more than 10% to the overall Auger intensity of this transition,[22] in agreement also with the above XPS results. Any attempt to include the ^1D multiplet term in the fit for the singles Auger spectrum, for which a sizable intensity is expected based on both theoretical calculation and experimental measurements of the $L_{23}M_{45}M_{45}$ decay,[11] resulted in destabilizing the convergence of the fitting procedure. Thus the trial function for the fitting reported in Fig. 1(b) consists of only four Voigt functions: the ^1G and the ^3F terms, for each of the spin-orbit split component (M_2 and M_3). The relative intensities of the different terms are further free parameters for each of the components. The position of the ^1G and ^3F terms of the M_3 component are also free parameters, while the corresponding terms of the M_2 component have been constrained to be 2.50 eV apart from the former, according to the SO separation obtained from the fit of the photoemission spectrum [see Fig. 1(a)]. The relative intensity between the M_3 and the M_2 components has been set equal to 0.5; such a constraint has been necessary due to the proximity of the ^3F term of the M_3 decay and the ^1G term of the M_2 decay that makes them strongly correlated in the fitting procedure. The statistical expected value (0.5) has been used, in spite of the BR measured between the $3p_{1/2}$ and $3p_{3/2}$ photoemission intensities as obtained by the XPS spectrum because the observed small deviation from 0.5 has been attributed to anisotropy effects of the escaping electrons and not to a different core-hole population which contributes to the intensity ratio between M_2 and M_3 decays. The thick solid line in Fig. 1(b) is the best fit to the experimental data, while the dash-dotted line is the estimated background. The ^1G-^3F splitting is 2.6 ± 0.7 eV, their Lorentzian width is 3.5 ± 0.3 eV, while the intensity ratio $^1G/^3F$ between the singlet and triplet terms is 2.1 ± 0.2.

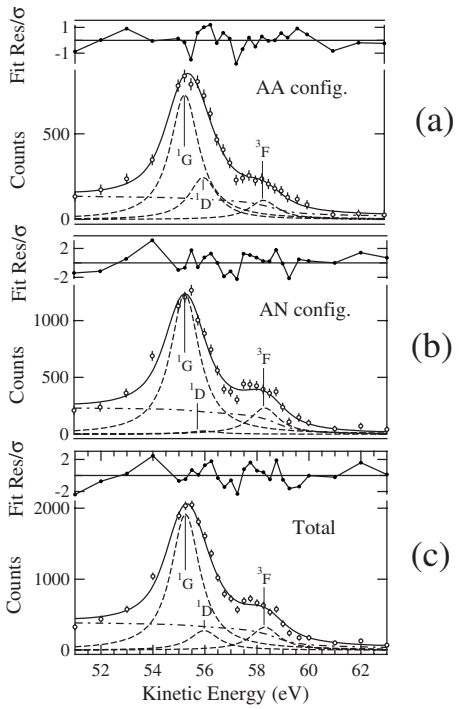

FIG. 2. Cu $M_3M_{45}M_{45}$ coincidence Auger spectra measured in configurations (a) *AA* and (b) *AN* and (c) their sum are reported as open circles with statistical error bars. The solid line is the best fit obtained by using the multiplet terms (dashed lines) describing the Auger transition (see text for more). Residuals relative to the error bars σ of each data point are shown in the top part of each panel.

The Auger spectra as measured in coincidence with $3p_{3/2}$ photoelectrons in configurations *AA* and *AN* are presented as open circles in Figs. 2(a) and 2(b), respectively, while the sum of the two spectra is shown in Fig. 2(c). This last spectrum is not simply the sum of the two previous spectra, but each energy point of it has been obtained by fitting the time spectrum given by the sum of the two-time spectra corresponding to the same energy point of the *AA* and *AN* configurations. In this respect, the resulting total coincidence spectrum has to be considered an independent statistical sampling of the APECS signal. Statistical error bars are reported together with the data. As measurements in coincidence with $3p_{3/2}$ photoelectrons discriminate the $3p_{3/2}$ decay path from that of the $3p_{1/2}$ core holes, these data refer to the M_3 transition only. Therefore coincidence experimental data have been fitted with a trial function (solid lines) made of three Voigt functions corresponding to the ^1G, ^1D, and ^3F multiplet terms (dashed lines) and a Shirley-type integral background (dash-dotted lines). The inclusion of the ^1D multiplet term, which was not possible to include in the singles data analysis, improved the reduced chi square and also the residual curve, which—by using only two multiplet terms (not shown)—displayed a lack of reliability in the *AA* data fit with a critical oscillation located in proximity of the ^1D multiplet term energy. The three spectra reported in Fig. 2 have been fitted simultaneously, that is, minimizing the chi square calculated over the three spectra together. The FWHM of the Gaussian broadening has been set equal or larger than 0.9 eV (indeed the obtained value remained unchanged and equal to

TABLE I. Experimental values of ^1G, ^1D, and ^3F relative splitting and intensities as obtained in singles (AES) and in the two geometrical configurations used for AR-APECS measurements. Relative intensities are compared with values obtained from the model.

Configuration	Linewidth (eV)	$^1G-^1D$ splitting (eV)	$^1G-^3F$ splitting (eV)	$^1G/^3F$	$^1D/^3F$
AES	3.5 ± 0.3	NA	2.6 ± 0.7	2.1 ± 0.2	NA
model				2.2	0.43
AR-APECS (*AA*)	1.34 ± 0.07	0.72 ± 0.14	3.01 ± 0.09	6.7 ± 0.7	2.2 ± 0.4
model				7.5	1.1
AR-APECS (*AN*)	1.34 ± 0.07	0.72 ± 0.14	3.01 ± 0.09	5.2 ± 0.4	0.1 ± 0.2
model				2.4	0.3

the energy resolution of the axial analyzers) and the Lorentzian width was a free parameter constrained to be equal for all the peaks. The energy splittings of the multiplet terms are forced to be equal for the three spectra, while the intensities of the peaks were free parameters. In the upper part of each panel the residuals are also shown, indicating the quality of the fit. It is evident that the coincidence Auger lineshape obtained in the *AA* configuration differs considerably from that obtained in the *AN* geometry. In particular, the relative contribution of the ^3F multiplet component suffers a sizable reduction in configuration *AA* [Fig. 2(a)] as compared to configuration *AN* [Fig. 2(b)]. In addition, the intensity of the ^1D component (kinetic energy around 56 eV) is negligible in configuration *AN*. These effects will be discussed in detail in Sec. IV and relative intensities are reported in Table I. The energy separation of the ^1D and the ^3F multiplet components with respect to the ^1G term are 0.72 ± 0.14 eV and 3.01 ± 0.09 eV, respectively. It is interesting to note that the background in the spectra of Fig. 2 is much reduced in comparison with its counterpart in the singles Auger spectrum [see Fig. 1(b)]. This effect has a twofold origin: (i) APECS enhances the surface sensitivity, thus reducing the probability of inelastic collisions for the electron pair, as discussed elsewhere;[23] (ii) most of the secondary electrons have no time correlation with the photoelectron and hence do not contribute to the coincidence signal. Finally, for APECS, the Lorentzian widths Γ_L are related to the lifetime of the core-hole state and to the delocalization time of the two final holes. The value obtained from the analysis of the coincidence Auger spectra ($\Gamma_L=1.34\pm0.07$ eV) is smaller than the one obtained from the analysis of the singles Auger spectra ($\Gamma_L=3.5\pm0.3$ eV). This reduction in the intrinsic energy width of the APECS spectrum has already been observed in other experiments.[22] In the present case, the difference between the two values is too large to be justified by the partial removal of the core-hole lifetime as well as by a selection of a subset among all the possible decays and will be discussed in Sec. IV.

In Fig. 3 the energy balance between photoelectrons and Auger electrons that arises by the coincident measurement is shown and quantitatively explained. In Fig. 3(a) we compare the coincidence Auger spectrum (open symbols and solid line) as obtained from the sum of the two configurations *AA* and *AN* [i.e., the one already shown in Fig. 2(c)] with the corresponding singles spectrum (dashed line) simultaneously collected. One sees that the kinetic-energy value of the intensity maximum (corresponding to the ^1G term) for APECS spectrum is shifted with respect to the corresponding singles spectrum by −0.5 eV. This observation can be explained considering energy conservation of the total process of photoemission followed by Auger decay. During acquisition of the APECS data presented here, photoelectron analyzers were set to collect electrons with a kinetic energy of 1.3 eV higher than the maximum of the $3p_{3/2}$ photoemission line, as collected with an energy resolution of 2.16 eV. In Fig. 3(b) the measured singles photoemission spectrum is shown as open circles along with the best fit obtained by using two

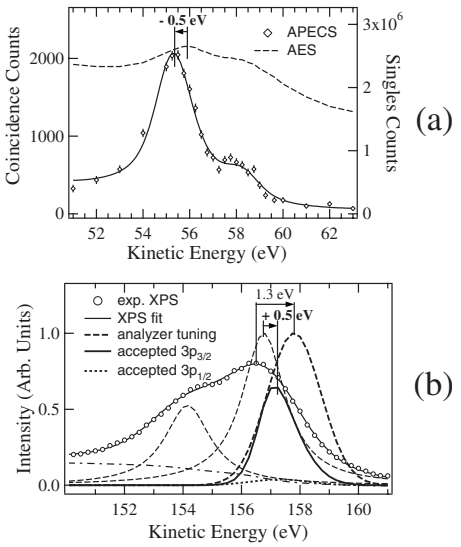

FIG. 3. Energy shifts occurring in APECS due to the energy conservation requirement. (a) Comparison between the Auger lineshape of the total coincidence spectrum (open rhombuses and fitting line) and the simultaneously acquired single Auger spectrum (dashed line). A shift in energy of about −0.5 eV between coincidence and single spectra is outlined. (b) Photoemission spectrum (open circles) superimposed with the best fit (thin solid line) with two Lorentzian components (thin dashed lines) and a Shirley-type integral background (dash-dotted lines). By multiplying each of the two Lorentzian peaks by the analyzer transmission curve (thick dashed line), one obtains the curves representing the accepted $3p_{3/2}$ photoelectrons (thick line) and the negligible amount of accepted $3p_{1/2}$ photoelectrons (thick dotted line). The former one results shifted by about +0.5 eV above the corresponding Lorentzian peak.

Voigt peaks corresponding to the two spin-orbit split components (thin-dashed lines). Here the component representing the $3p_{3/2}$ term has been arbitrarily normalized to unity. The curve shown as a thick-dashed line is a Gaussian with a FWHM of 2.16 eV, centered 1.3 eV higher than the photoemission spectrum maximum, representing the energy window collected by the photoelectron analyzer. Multiplying this Gaussian window with the Lorentzian photoelectron energy distribution, one obtains the distribution of the $3p_{3/2}$ ($3p_{1/2}$) photoelectrons which are finally accepted in the coincidence measurement shown as thick solid line (thick-dotted line) in Fig. 3(b). This analysis shows that the distribution of accepted $3p_{3/2}$ photoelectrons is centered +0.5 eV above the peak in the $3p_{3/2}$ line and has a FWHM of 1.5 eV. Since in the coincidence process, energy is conserved collectively by the coincidence electron pair, if higher-energy photoelectrons are selected, Auger electrons originating from the same core ionization event must have an energy lower than the diagrammatic value. This explains why the coincidence Auger spectrum is shifted by −0.5 eV to lower energy with respect to the singles Auger distribution displayed in Fig. 3(a). This result is in agreement with previous findings,[22] where a linear dispersion of the coincidence photoline as a function of the Auger-electron energy was observed and is a confirmation of the one-step character of the event composed by the photoionization process and the subsequent Auger decay. This is a general rule for coincidence measurements,[33] where more than one particle are measured and has been observed also in discussing the CK satellite structure in a coincidence experiment between the Cu $L_{23}M_{45}M_{45}$ Auger electrons and the Cu $2p_{1/2}$ photoelectrons. In such a case the energy conservation applied to three particles has been used,[43] that is, including also the electron emitted by the CK decay. Therefore attention must be paid whenever considering the exact energy position of the measured spectroscopic features. For instance, in another APECS measurement where the Cu $2p_{3/2}$ has been measured in coincidence with the Cu $L_3M_{45}M_{45}$ Auger main peaks, it has been speculated[44] that the energy shift observed in the photoemission peak could be attributed to two different bandlike versus atomiclike behaviors of the two ^1G an ^3F multiplet terms that give rise to two components (bandlike and atomiclike) also in the photoemission peak. As a matter of fact, if we recall that the L_3 core-hole lifetime broadening is much smaller than that of the M_3 level and that such an energy conservation effect can be applied only within an energy window determined by the core-hole lifetime broadening [i.e., where the decay signal exists], we conclude that a smaller—and therefore more difficult to quantify—effect is expected for the $L_3M_{45}M_{45}$ decay with respect to what is measured in the present work on the $M_3M_{45}M_{45}$ Auger spectrum.

IV. DISCUSSION

The observed differences in the energy distribution of the Auger electrons, in terms of different relative intensities of the multiplet terms when measured in the two different geometric configurations, can be explained by using a model where the entire process is described in two steps: emissions from the atomic site (photoemission and Auger-electron emission) and electron diffraction by the crystal. Within this approach the photoelectron and the Auger-electron-diffraction patterns are generated once the atomic wave functions of the ejected electron—the so-called "source waves"—are diffracted by the crystal lattice.[45,46] Regarding the role played by diffraction, for high kinetic-energy electrons ($E_k > 300$ eV), forward scattering is dominant in determining their angular distribution, while at lower energies large-angle scattering is also important. As atomic scattering will influence the anisotropy of the pattern while leaving almost unaffected the memory on the quantum numbers dictated by the atomic source wave function,[47] large-angle scattering will probably diffuse different sublevels at distinct angles in a more efficient way with respect to forward focusing.[48] To discuss the shape of the energy spectra presented in Sec. III, one must consider which partial waves are allowed for the continuum electrons and evaluate their relative contributions to emission at the various angles at which the photoelectron and Auger electron will be detected. Anisotropy of the source waves as determined by core-hole polarization is accounted for by the introduction of a quantization axis along the polarization axis of the incident light. In the case of linear polarization, the core-hole ion can only be aligned along this direction with equal populations for $\pm m$, where m is the magnetic quantum number for projection along the quantization axis.

In order to characterize the source wave, we have to consider the selection rules governing photoionization and subsequent decay. In the case of photoexcitation, the optical dipole selection rules reduce to $\Delta l = \pm 1$ the possible partial waves of the photoelectrons (where Δl is the change of the angular-momentum quantum number l). Moreover, linearly polarized light implies $\Delta m = 0$. As a result the m values of the photoelectrons are identical to those of the core hole left behind. On the other hand, the quantum numbers of the core hole enter into the selection rules for the Auger decay process according to the following expressions:[49]

$$l_c + l_1 + \kappa = \text{even integer}, \tag{1}$$

$$l_A + l_2 + \kappa = \text{even integer}, \tag{2}$$

$$\beta = m_1 - m_c = m_A - m_2, \tag{3}$$

$$|l_c - \kappa| \leq l_1 \leq l_c + \kappa, \tag{4}$$

$$|l_A - \kappa| \leq l_2 \leq l_A + \kappa, \tag{5}$$

where l_c, l_A, l_1, and l_2 are the orbital quantum numbers of the core hole, the emitted Auger electron, and the two holes left after the Auger-electron emission, respectively. Similarly, m_c, m_A, m_1, and m_2 are the corresponding magnetic quantum numbers. κ and $\beta = \{-\kappa, -\kappa+1, \ldots, 0, \ldots, \kappa-1, \kappa\}$ are, respectively, the orbital and magnetic quantum numbers related to the expansion of the Coulomb interaction in spherical harmonics (see Ref. 49 for details). Since in this experiment a $3p$ level is ionized, $l_c = 1$, the photoelectron will have either $l_p = 0$ (s wave) or $l_p = 2$ (d wave) and only final states with $m_c \equiv m_p = 0, \pm 1$ can be accessed (l_p and m_p are the orbital

and magnetic quantum numbers of the photoelectrons, respectively). Moreover, as the measurements are performed on the $M_3M_{45}M_{45}$ Auger transition, the final state contains two holes in a d level and therefore $l_1=l_2=2$. Furthermore, previous studies of similar transitions indicate that the emerging Auger electron is predominantly of f-wave character ($l_A=3$),[45,46] thus the possible values of the magnetic quantum number are limited to $m_A=0,\pm1,\pm2,\pm3$.

In the atomic case, photoelectron and Auger-electron angular distributions can be obtained using the well-known density-matrix and statistical tensors formalism,[50] where they are given by tensorial products of spherical harmonics, describing the angular contribution for each partial wave weighted by the angle-dependent components of the statistical tensors, which describe the core-hole polarization. In the present case, spherical harmonics with $m=0$ are the only ones contributing along the normal to the surface while the spherical harmonic Y_{31}, for example, which describes a possible channel for the Auger electron, has a maximum around 40° from the surface normal. Thus by modifying the angle of detection of the two electrons, it is possible to enhance or suppress the measured intensity originated from the contribution of determined sublevels.

Now, when analyzing electron emission from solids, diffraction effects must be taken into account. Electrons coming from different multiplet terms of the decay can give rise to different diffraction patterns since they have slightly different energies and different partial-wave expansions. Let us consider the latter dependence expressed in terms of the quantum numbers of the emitted electrons as suggested by Refs. 45 and 46. Simulations of diffraction based on the multiple-scattering calculation of diffraction (MSCD) code[51] modified for extracting individuals m contributions are shown in Fig. 4(a) for a specific azimuthal angle appropriate for the photoelectrons of interest, while those relevant for Auger electrons are shown in Figs. 4(b) and 4(c) corresponding to two azimuthal angles appropriate for Auger electrons of interest. The MSCD code simulates the electron-diffraction patterns from a solid on the base of the Rehr-Albers separable representation of spherical propagators[52] and calculations are performed using a muffin-tin potential. We used the kinetic energies of 56 and 156 eV for the Auger $M_3M_{45}M_{45}$ and the $3p$ core level, respectively, and the multiple-scattering order was 8 with a Rehr-Albers order 2. The cluster size was of about 300 atoms, with an inner potential $V_0=7.5$ eV and a Debye temperature of 350 K. The potential, the phase shifts, and the radial matrices needed for the calculations have been obtained within the MSCD package. As $M_3M_{45}M_{45}$ emitted Auger electrons have predominantly f-wave character, the angular distribution is modeled by dipole excitation of d level (i.e., $l=2$) and allowing only the $l+1$ (i.e., $l=3$) channel in the final state. From Fig. 4 we can observe that in accordance to what has been already pointed out in Refs. 45 and 46, each magnetic sublevel contributes to the total intensity with different relative weight at the different scattering angles [the $m_A=\pm3$ contributions are not included in Figs. 4(b) and 4(c) and in the following discussion since they are thought to be much less intense than the others]. Therefore in an AR-APECS experiment, the electron analyzers, which are set at specific detection angles, will

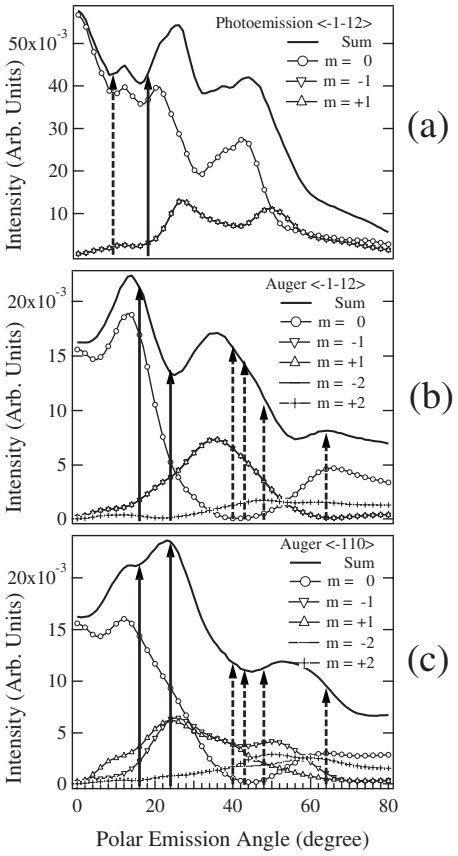

FIG. 4. m resolved electron-diffraction simulations with the MSCD code. The photoelectron polar distribution is shown in (a) at an azimuthal angle corresponding to the $\langle\bar{1}\bar{1}2\rangle$ direction. Two Auger-electron polar distributions are shown in (b) and (c) along the $\langle\bar{1}\bar{1}2\rangle$ and $\langle\bar{1}10\rangle$ azimuthal directions, respectively. The total intensity (thick solid line) and the partial intensities for waves having $m=0$ (open circles and line), $m=-1$ (open down triangles and line), $m=1$ (open up triangles and line), $m=-2$ (minus symbols and line), and $m=2$ (plus symbols and line) are plotted as a function of the polar emission angle. Solid and dashed arrows indicate the positions of the analyzers in configurations AA and AN, respectively.

preferentially detect electrons characterized by particular quantum numbers rather than by others. On the other hand, selecting particular orbital and magnetic quantum numbers of the two emitted electrons results in selecting different contributions for the two-hole final state, whose combinations determine the multiplet structure of the Auger spectrum. In other words, selectivity toward the magnetic quantum numbers involved in the transition can be achieved through choosing appropriated detection conditions.

For the sake of simplicity, let us now consider the contribution to the overall intensity due to the terms in the Coulomb expansion for which $\beta=0$. Then Eq. (3) reduces to the simple condition $m_p=m_1$ and $m_A=m_2$. It is evident from Fig. 4 that near the surface normal, the $m=0$ contribution is dominant both for photoelectrons and Auger electrons. The solid (dashed) arrows in the figure indicate the position of the analyzers in configuration AA (AN). Thus configuration AA, in which both photoelectron and Auger electron are detected closer to the normal, enhancement of the $m=0$ contribution

for both the photoelectron and the Auger electrons is expected. Consequently the $m_1=m_2=0$ condition is favored in the two-hole final state. In such case, taking into account that the orbital angular-momentum quantum numbers l_1 and l_2 are the same since the two holes are both in a d level, the intensity of the ^3F multiplet term is zero. This is the case because the Pauli exclusion principle prohibits two holes in the same level with all the same quantum numbers. The simulations of Fig. 4 also indicate that contributions from other sublevels are not zero at the detection angles of configuration *AA*, particularly, for the positions of the analyzers detecting the Auger electrons. Thus, in practice, in configuration *AA* we are not revealing only the $m=0$ contribution, but we are detecting electrons characterized by a mixture of states given by all the allowed magnetic quantum numbers m among which the $m=0$ component is dominant. Therefore the ^3F term does not vanish completely but its intensity is greatly reduced, leading to $^1G/^3F$ and $^1D/^3F$ ratios that are greater in configuration *AA* than in other geometrical conditions where the $m=0$ contribution is less important. The curves of Fig. 4 also show that the $m\geq 1$ contributions are zero at normal emission for both the photoelectron and the Auger electron and become dominant at larger angles, where the $m_A=0$ contribution is less important. In the geometrical condition of configuration *AN*, the bimodal analyzers were positioned close to the surface normal, while the axial analyzers were at polar angles $\geq 40°$. Thus, according to the results of Fig. 4, this experimental setup was selecting essentially electrons characterized by $m_p=0$ and $m_A\geq 1$, where the total diffraction pattern would actually be an admixture of the different contributions with their own relative weights. In contrast to configuration *AA*, we therefore expect that in configuration *AN* the ^1G contribution is less favored (since $m_1\neq m_2$ and the ^3F term does not vanish), leading to $^1G/^3F$ and $^1D/^3F$ ratios that are smaller in configuration *AN* than in configuration *AA*. This is indeed the qualitative result one observes by comparing Figs. 2(b) and 2(c). Such changes in the coincidence spectra indicate that owing to the different spatial orientations of the fivefold-degenerate d orbitals and the threefold-degenerate p orbitals involved in the process, different contributions from the magnetic sublevels can be observed for particular geometrical conditions.

Similar considerations could be applied for the other terms in the Coulomb expansion. Thus, by properly combining selection rules with partial-waves anisotropies, it should be possible to correctly estimate the relative weight of the multiplet terms. But in such cases the simple rules $AA\rightarrow$singlet enhancing and $AN\rightarrow$triplet enhancing will not be valid anymore. Therefore, in order to keep a description of the multiplet term selectivity as much simple as possible, we have neglected these higher-order contributions obtaining anyway a good qualitative agreement with the experiment.

In order to obtain a more quantitative interpretation of these considerations, it is possible to estimate the contributions to the coincidence lineshape from each sublevel selected by the different analyzers by using the results of the diffraction calculations reported in Fig. 4. The simulations of Fig. 4 show diffraction patterns for only some selected azimuthal angles. The important qualitative result is that the $m=0$ component is dominant at small polar angles, while at larger polar angles waves with $m>0$ become more important. The results of the simulation are used for comparing our simple model with the experiment without concerning to the exact azimuthal angle, obtaining in any case a qualitative good agreement. The Auger lineshape measured in coincidence can be derived writing the related intensity I as a linear combination of lineshapes weighted by these different contributions,

$$I=\sum_{m_p=-1}^{1} I_{m_p}(\theta,\phi)\sum_{m_A=-2}^{2} I_{m_A}(\theta,\phi)\Gamma_{m_p m_A}, \tag{6}$$

where $\Gamma_{m_p m_A}$ are Lorentzian functions chosen to describe the lineshape of an individual component (for $m_p=0,\pm 1$ and for $m_A=0,\pm 1,\pm 2$) and $I_{m_p=0,1}$ and $I_{m_A=0,1,2}$ are the intensities of the different sublevels derived from the diffraction patterns of Fig. 4, estimated at the polar θ and azimuthal ϕ emission angles chosen for the experiment. The $\Gamma_{m_p m_A}$ terms can be written as

$$\Gamma_{m_p m_A}=\sum_{^{2S+1}L=^1G,^1D,^3F}\Pi_{m_p m_A}(^{2S+1}L)\frac{\gamma}{\pi[(x-x_{^{2S+1}L})^2+\gamma^2]}, \tag{7}$$

where $\Pi_{m_p m_A}(^{2S+1}L)$ is given by the product of the Clebsch-Gordan coefficient of that particular combination of m_p and m_A by the transition probability related to the multiplet term ^{2S+1}L. In this way, the Auger coincidence lineshape has been built for the dominant multiplet terms in the spectrum taking the atomic contributions for each magnetic sublevels weighted by the "diffraction effects," i.e., by the relative weights for specific detection angles. Thus it is possible to derive the values of the $^1G/^3F$ and $^1D/^3F$ ratios for different polar angles and compare them to the experimental results obtained in the two different configurations (see Fig. 2). These calculated ratios together with relative energy splittings and linewidths are reported in Table I and compared with experimental values obtained for both the AR-APECS and conventional AES measurements. Good qualitative agreement can be seen, and we can therefore state that changes in the geometrical conditions of the experiment change the lineshape in the coincidence spectrum in accordance with the behavior expected from the model. Thus, depending on the relative orientation of the light polarization and the two linear momenta of the continuum electrons, the alignment of the core-hole ionization state changes and—despite of diffraction effects—it results to be essential to determine the details of the lineshape itself.

It is interesting to note that the experimental evidence that APECS selects more efficiently the ^1G term with respect to singles in both *AA* and *AN* configurations and not only in the *AA* one as it is expected by the calculation (see Table I) indicates that the multiplet term selectivity is not perfectly reproduced by the model if only the terms with $\beta=0$ are included in the Coulomb expansion. Therefore, it is reasonable to think that the overall effect of including all the higher-order terms with $\beta>0$ evaluated for these two geometries should be to slightly favor the ^1G term. This effect notwithstanding, the contrast observed on the relative inten-

sity of the multiplet terms achieved by comparing the two configurations *AA* and *AN* is high enough to acquire reliable spectroscopic information on the Cu $M_3M_{45}M_{45}$ Auger decay.

Moreover, if on one hand also single spectra (AES) should display an angular dependence in their lineshapes—as can be easily accounted for in the theory,[42] on the other hand, by fitting the experimental AES spectra, there is no possibility to obtain the correct relative intensities of the multiplet terms. This is due to the overlap between multiplet terms of the M_2 and M_3 decays channels and to the large core-hole lifetime broadening which bring to a poor quality data fitting, even when introducing more constraints as was done in fitting the singles spectrum in Fig. 1(b) and even if the energy resolution was better than in coincidence measurements. This lack of reliability in AES may be the motivation why a so-high Lorentzian width of the Auger multiplet terms has been observed in singles with respect to coincidence data, well beyond the difference expected by the line narrowing due to the partial removal of the core-hole lifetime broadening achieved by the coincidence detection.

Finally, the different intensity ratios between multiplet terms having different spin character measured in the two AR-APECS configurations amount to a "geometrically induced dichroism"[27] resulting from discrimination among the magnetic sublevels achieved by angle selection.

V. CONCLUSIONS

In this work, the capability of AR-APECS to control the measured contribution of different multiplet components to an Auger spectrum has been applied for the study of the Cu $M_3M_{45}M_{45}$ Auger decay. This has been related to the selectivity in the magnetic quantum number invoked by the angle-resolved detection, which allows one to observe different contributions from the sublevels even if they are energetically degenerate. In this way, a reliable experimental estimation of the energy and intensity for the ^1D term has been provided. While the development of a precise theory is necessary to fully understand the results, a simple model, where the sublevel populations are taken at different detection angles and weighted by Auger transition matrix elements and diffraction effects, already accounts for most of the observed effect. In the present case, it is the selection of a particular core-hole polarization that determines the anisotropy of the angular distributions and the weights of the different continuum channels of the Auger electrons measured in coincidence. On the other hand, such a unique capability of APECS to investigate the population of magnetic sublevels may open the possibility to investigate systems with non-statistical distributions of the magnetic quantum number such as magnetic materials. Furthermore, considering the high-surface sensitivity or the capability of AR-APECS to discriminate among the electrons emitted from different atomic layers, the technique could study magnetic nanostructures with unprecedented localization capability. Finally, since single-particle local DOS is actually obtained fully *ab initio* in the framework of density-functional theory (only the hole-hole screening interaction is a free parameter) and the CS theory can be used to model the spectra with the aim of properly considering a spin-dependent electronic correlation effects,[42] AR-APECS is the experimental technique best suited to act as a stringent test.

ACKNOWLEDGMENTS

The authors are grateful to the ALOISA beamline staff members for the valuable support provided during the AR-APECS experiments performed at the ELETTRA synchrotron-radiation facility. Financial support from the MIUR PRIN 2005 contract "Studio di sistemi ad alta correlazione e bassa dimensionalitá con spettroscopie di coincidenza: una nuova generazione di metodi sperimentali e teorici" and from INFM program "Supporto utenti luce di sincrotrone" is gratefully acknowledged. F.O. acknowledges the support of the European Community under Contract No. HPRI-CT-2001-50032, two of us (H.Y. and R.A.B.) acknowledge support from the NSF under Grant No. DMR98-01681, and A.V. acknowledges F. Bondino for the hints in modifying the MSCD codes.

*Present adress: Institut Carnot de Bourgogne, UMR 5209 CNRS-Université de Bourgogne, BP 47870, 21078 Dijon Cédex, France.

[1] Raman resonant Auger spectroscopy and Auger-photoelectron coincidence spectroscopy using synchrotron radiation are two examples; see, for example, George S. Brown, Mau Hsiung Chen, Bernd Crasemann, and Gene E. Ice, Phys. Rev. Lett. **45**, 1937 (1980); M. Weinelt, A. Nilsson, M. Magnuson, T. Wiell, N. Wassdahl, O. Karis, A. Fohlisch, N. Mårtensson, J. Stohr, and M. Samant, *ibid.*only **78**, 967 (1997).

[2] R. A. Bartynski, E. Jensen, S. L. Hulbert, and C.-C. Kao, Prog. Surf. Sci. **53**, 155 (1996).

[3] M. I. Trioni, S. Caravati, G. P. Brivio, L. Floreano, F. Bruno, and A. Morgante, Phys. Rev. Lett. **93**, 206802 (2004).

[4] P. Weightman, Rep. Prog. Phys. **45**, 753 (1982).

[5] S. P. Kowalczyk, R. A. Pollak, F. R. McFeely, L. Ley, and D. A. Shirley, Phys. Rev. B **8**, 2387 (1973).

[6] P. Weightman, J. F. McGilp, and C. E. Johnson, J. Phys. C **9**, L585 (1976).

[7] L. I. Yin, I. Adler, T. Tsang, M. H. Chen, D. A. Ringers, and B. Crasemann, Phys. Rev. A **9**, 1070 (1974).

[8] E. D. Roberts, P. Weightman, and C. E. Johnson, J. Phys. C **8**, L301 (1975).

[9] E. J. McGuire, Phys. Rev. A **16**, 2365 (1977).

[10] P. J. Feibelman and E. J. McGuire, Phys. Rev. B **15**, 3575 (1977).

[11] E. Antonides, E. C. Janse, and G. A. Sawatzky, Phys. Rev. B **15**, 1669 (1977).

[12] E. J. McGuire, Phys. Rev. A **17**, 182 (1978).

[13] C. F. Hague, J.-M. Mariot, and H. Ostrowiecki, Jpn. J. Appl. Phys. **17** (Supplement 17–2), 105 (1978); H. Guennou, A.

Sureau, G. Dufour, C. F. Hague, and J.-M. Mariot, in *Inner-Shell and X-Ray Physics of Atoms and Solids*, edited by D. J. Fabian, H. Kleinpoppen, and L. M. Watson (Plenum, New York, 1981) p. 797; S. Aksela and J. Sivonen, Phys. Rev. A **25**, 1243 (1982).
[14] M. Cini, Solid State Commun. **24**, 681 (1977).
[15] G. A. Sawatzky, Phys. Rev. Lett. **39**, 504 (1977).
[16] H. W. Haak, G. A. Sawatzky, and T. D. Thomas, Phys. Rev. Lett. **41**, 1825 (1978).
[17] D. D. Sarma, S. R. Barman, R. Cimino, C. Carbone, P. Sen, A. Roy, A. Chainani, and W. Gudat, Phys. Rev. B **48**, 6822 (1993).
[18] D. D. Sarma, S. R. Barman, C. Carbone, R. Cimino, W. Eberhardt, and W. Gudat, J. Electron Spectrosc. Relat. Phenom. **93**, 181 (1998).
[19] I. Coulthard, T. K. Sham, Y.-F. Hu, S. J. Naftel, P.-S. Kim, and J. W. Freeland, Phys. Rev. B **64**, 115101 (2001).
[20] W. Drube, R. Treusch, and G. Materlik, Phys. Rev. Lett. **74**, 42 (1995).
[21] T. K. Sham, A. Hiraya, and M. Watanabe, Phys. Rev. B **55**, 7585 (1997).
[22] E. Jensen, R. A. Bartynski, S. L. Hulbert, E. D. Johnson, and R. Garrett, Phys. Rev. Lett. **62**, 71 (1989).
[23] A. Liscio, R. Gotter, A. Ruocco, S. Iacobucci, A. G. Danese, R. A. Bartynski, and G. Stefani, J. Electron Spectrosc. Relat. Phenom. **137-140**, 505 (2004).
[24] W. S. M. Werner, W. Smekal, H. Störi, H. Winter, G. Stefani, A. Ruocco, F. Offi, R. Gotter, A. Morgante, and F. Tommasini, Phys. Rev. Lett. **94**, 038302 (2005).
[25] G. Stefani, R. Gotter, A. Ruocco, F. Offi, F. Da Pieve, S. Iacobucci, A. Morgante, A. Verdini, A. Liscio, H. Yao, and R. A. Bartynski, J. Electron Spectrosc. Relat. Phenom. **141**, 149 (2004); G. Stefani, R. Gotter, A. Ruocco, F. Offi, F. Da Pieve, A. Verdini, A. Liscio, S. Iacobucci, H. Yao, and R. A. Bartynski, in *Correlation Spectroscopy of Surfaces, Thin Films, and Nanostructures*, edited by J. Berakdar and J. Kirschner (Wiley, Weinheim, 2004), p. 222.
[26] R. Gotter, A. Ruocco, M. T. Butterfield, S. Iacobucci, G. Stefani, and R. A. Bartynski, Phys. Rev. B **67**, 033303 (2003).
[27] R. Gotter, F. Da Pieve, A. Ruocco, F. Offi, G. Stefani, and R. A. Bartynski, Phys. Rev. B **72**, 235409 (2005).
[28] J. Berakdar and S. Mazevet, J. Phys. B **32**, 3965 (1999).
[29] K. Soejima, M. Shimbo, A. Danjo, K. Okuno, E. Shigemasa, and A. Yagishita, J. Phys. B **29**, L367 (1996).
[30] J. Berakdar, J. Phys. B **31**, 3167 (1998).
[31] R. Gotter, F. Offi, F. Da Pieve, A. Ruocco, G. Stefani, S. Ugenti, M. I. Trioni, and R. A. Bartynski, J. Electron Spectrosc. Relat. Phenom. **161**, 128 (2007).
[32] R. Gotter, A. Ruocco, A. Morgante, D. Cvetko, L. Floreano, F. Tommasini, and G. Stefani, Nucl. Instrum. Methods Phys. Res. A **467-468**, 1468 (2001).
[33] G. A. Sawatzky, in *Auger Photoelectron Coincidence Spectroscopy, Treatise on Material Science and Technology*, edited by C. L. Briant and R. P. Messmer, Academic, New York, 1988), Vol. 30, pp. 167–243.
[34] Ch. Gerth, K. Tiedtke, M. Martins, B. Obst, P. Zimmermann, P. Glatzel, A. Verweyen, Ph. Wernet, and B. Sonntag, J. Phys. B **31**, 2539 (1998).
[35] J. C. Fuggle, E. Källne, L. M. Watson, and D. J. Fabian, Phys. Rev. B **16**, 750 (1977).
[36] A. Lebugle, U. Axelsson, R. Nyholm, and N. Mårtensson, Phys. Scr. **23**, 825 (1981).
[37] Ch. Roth, F. U. Hillebrecht, W. G. Park, H. B. Rose, and E. Kisker, Phys. Rev. Lett. **73**, 1963 (1994).
[38] W. R. A. Huff, Y. Chen, S. A. Kellar, E. J. Moler, Z. Hussain, Z. Q. Huang, Y. Zheng, and D. A. Shirley, Phys. Rev. B **56**, 1540 (1997); The SO value has been deduced from Fig. 1(b).
[39] H. W. Yeom, T. Abukawa, Y. Takakuwa, S. Fujiimori, T. Okane, Y. Ogura, T. Miura, S. Sato, A. Kakizaki, and S. Kono, Surf. Sci. **395**, L236 (1998).
[40] M. T. Sieger, T. Miller, and T.-C. Chiang, Phys. Rev. Lett. **75**, 2043 (1995).
[41] J. C. Slater, *Quantum Theory of Atomic Structure* (McGraw-Hill, New York, 1960), Vol. 2, pp. 286 and 294.
[42] S. Ugenti, M. Cini, E. Perfetto, F. Da Pieve, C. Natoli, R. Gotter, F. Offi, A. Ruocco, G. Stefani, F. Tommasini, G. Fratesi, M. I. Trioni, and G. P. Brivio, J. Phys.: Conf. Ser. **100**, 072020 (2008).
[43] S. M. Thurgate, C. P. Lund, C. Creagh, and R. Craig, J. Electron Spectrosc. Relat. Phenom. **93**, 209 (1998).
[44] S. M. Thurgate and Z.-T. Jiang, Surf. Sci. **466**, L807 (2000); We tried to repeat the experiment on the Cu $L_3M_{45}M_{45}$ Auger decay with a better energy resolution but we didn't observe the same effect.
[45] Y. U. Idzerda, Surf. Rev. Lett. **4**, 161 (1997).
[46] D. E. Ramaker, H. Yang, and I. U. Idzerda, J. Electron Spectrosc. Relat. Phenom. **68**, 63 (1994).
[47] Ph. Wernet, J. Schulz, B. Sonntag, K. Godehusen, P. Zimmermann, M. Martins, C. Bethke, and F. U. Hillebrecht, Phys. Rev. B **62**, 14331 (2000).
[48] F. Da Pieve, D. Sébilleau, S. Di Matteo, R. Gunnella, R. Gotter, A. Ruocco, G. Stefani, and C. R. Natoli, Phys. Rev. B **78**, 035122 (2008).
[49] P. J. Feibelman, E. J. McGuire, K. C. Pandey, and P. Weightman, Phys. Rev. B **15**, 2202 (1977); G. Cubiotti, A. Laine, and P. Wieghtman, J. Phys.: Condens. Matter **1**, 7723 (1989); E. J. McGuire, in *"Auger and Coster-Kronig Transitions," in Atomic Inner-Shell Processes*, edited by B. Crasemann (Academic, New York, 1975), pp. 293–330.
[50] N. M. Kabachnik, J. Phys. B **25**, L389 (1992).
[51] See http://www.ap.cityu.edu.hk/personal-website/VanHove_files/mscd/mscdpack.html.
[52] J. J. Rehr and R. C. Albers, Phys. Rev. B **41**, 8139 (1990).